Published in final edited form as:
J Am Chem Soc. 2009 September 16; 131(36): 12979–12988. doi:10.1021/ja902473r.

Direct Detection of the Oxygen Rebound Intermediates, Ferryl Mb and NO_2, in the Reaction of metMyoglobin with Peroxynitrite

Jia Su and **John T. Groves***
Department of Chemistry, Princeton University, Princeton NJ 08544

Abstract

Oxygenated hemoproteins are known to react rapidly with nitric oxide (NO) to produce peroxynitrite (PN) at the heme site. This process could lead either to attenuation of the effects of NO or to nitrosative protein damage. Peroxynitrite is a powerful nitrating and oxidizing agent that has been implicated in a variety of cell injuries. Accordingly, it is important to delineate the nature and variety of reaction mechanisms of PN reactions with heme proteins. Here we present direct evidence that ferrylMb and NO_2 are both produced during the reaction of PN and metmyolgobin (metMb). Kinetic evidence indicates that these products evolve from initial formation of a caged radical intermediate [Fe^{IV}=O $\cdot NO_2$]. This caged pair reacts mainly via internal return with a rate constant k_r to form metMb and nitrate in an oxygen rebound scenario. Detectable amounts of ferrylMb are observed by stopped-flow spectrophotometry, appearing at a rate consistent with the rate, k_{obs}, of heme-mediated PN decomposition. Freely-diffusing NO_2, which is liberated concomitantly from the radical pair (k_e), preferentially nitrates Tyr103 in horse heart myoglobin. The ratio of the rates of in-cage rebound and cage escape, k_r/k_e, was found to be ~10 by examining the nitration yields of fluorescein, an external NO_2 trap. This rebound/escape model for the metMb/PN interaction is analogous to the behavior of alkyl hyponitrites and the well-studied geminate recombination processes of deoxymyoglobin with O_2, CO and NO. The scenario is also similar to the step-wise events of substrate hydroxylation by cytochrome P450 and other oxygenases. It is likely, therefore, that the reaction of metMb with $ONOO^-$ and that of oxyMb with NO proceed through the same [Fe^{IV}=O $\cdot NO_2$] caged radical intermediate and lead to similar outcomes. The results indicate that while oxyMb may reduce the concentration of intracellular NO, it would not eliminate the formation of NO_2 as a decomposition product of peroxynitrite.

Introduction

Although myoglobin (Mb) is a textbook paradigm for mediating oxygen storage and delivery in vertebrate skeletal and cardiac muscle tissue,[1] important alternative roles as an intracellular nitric oxide (NO) dioxygenase[2,3] and a nitrite reductase[4,5] have been recognized only recently. These discoveries have offered many new insights regarding this “old” protein. Nitric oxide (NO) is a central signaling device for both intra- and intercellular communication.[6] Considering the large amounts of oxyMb in normoxic muscle cells and the compartmentalization of NO production, the scavenging and degradation of NO by oxyMb is probably an important pathway

John T. Groves, Department of Chemistry, Princeton University, Princeton, New Jersey 08544, Phone: (609) 258-3593, Fax: (609) 258-0348, jtgroves@Princeton.EDU.

Supporting Information Available. Kinetic plots for ferrylMb reduction catalyzed by ascorbate; kinetic plots for ferrylMb reduction by peroxynitrite; Mass spectra of metMb/PN reaction mixture; additional equations used in the mechanistic simulations; experimental and simulated nitrofluorescein formation and concurrent PN decomposition in the absence of proteins; simulations of intermediate **I** formation and decay in the absence and presence of fluorescein. This material is available free of charge via the Internet at http://pubs.acs.org

to attenuate the spatial range of these signals. Conversely, the Mb reaction with nitrite to produce NO may be important under hypoxic conditions.[4,7]

Peroxynitrite (PN) evolves *in vivo* from the very fast combination of superoxide ion ($O_2^{\cdot -}$) and NO, as a consequence of aerobic metabolism and overproduction of NO.[8,9] Since both peroxynitrite anion ($ONOO^-$) and peroxynitrous acid (HOONO) can diffuse readily across biomembranes,[10,11] PN exhibits a wide range of reactivity in the modifications of many cellular targets, through one- and two-electron oxidations, nitrosation and nitration of various protein residues.[12,13] Heme proteins, such as myoglobin, [14,15] hemoglobin,[16,17] peroxidases,[18-20] cytochrome *c*,[21,22] nitric oxide synthase,[23] cytochrome P450[24] and the newly discovered neuroglobins[25] have all been observed to interact with PN and mediate its decomposition.

The reaction of PN with ferric myoglobin (metMb), and the concomitant nitration of protein tyrosine have been reported.[14,26,27] However, there is no consensus regarding the mechanism of the metMb/PN interaction and, especially, the identification of intermediates formed in the course of the reaction. Herold et al. have provided evidence that the reaction between oxyMb with NO leads to the formation of an intermediate $MbFe^{III}$-OONO adduct, which ultimately affords metMb and NO_3^-,[28,29] although the $MbFe^{III}$-nitrato complex has been shown to exhibit similar kinetics.[30] We have suggested a mechanism for the PN-metMb reaction that involves a protein-caged ferryl intermediate [Fe^{IV}=O $\cdot NO_2$] deriving from the facile O-O bond homolysis of $MbFe^{III}$-O-ONO (Scheme 1).[14] The ferryl intermediate has not been unequivocally identified during the oxyMb-NO reaction, although there is suggestive epr evidence for this process.[31,32] Reactions of PN with water-soluble Fe^{III} and Mn^{III} porphyrins have been reported by us[33-37] and by the Monsanto group.[38] Both Fe^{III}TMPS and Fe^{III}TMPyP react rapidly with $ONOO^-$ to produce ferryl intermediates.[34,35] Likewise, the reactions of PN with CYP 119[39] and myeloperoxidase[20] also lead to build-up of the ferryl species.

In the current work, we have used kinetic and spectroscopic techniques to interrogate the interaction between metMb and PN, building on our previously reported studies.[14] The results show that metMb reacts rapidly with PN to form the ferryl species, $MbFe^{IV}$=O, which has been spectroscopically identified and kinetically characterized. Further, we employed fluorescein as a trap of freely-diffusing NO_2 and nano-LC-ESI-MS/MS to confirm that the specific nitration site is Tyr103. Combined with the measured rate constant of ferrylMb formation in the course of PN decay, the results support a mechanism involving a [$MbFe^{IV}$=O $\cdot NO_2$] radical pair that dissociates to free $MbFe^{IV}$=O and $\cdot NO_2$ or collapses to $MbFe^{III}$ and nitrate ion, in a scenario that is analogous to myoglobin-ligand (NO, CO and O_2) geminate recombination and cage escape.[40,41]

Results

Direct detection of ferryl Mb (I) formed during the reaction of metMb with PN

PN decomposition was examined by studying the absorbance decay of PN anion at 302 nm by stopped-flow spectrophotometry as we have previously described.[14] The inventory of heme species formed during the reaction of metMb with PN was monitored in the stopped-flow device over the course of PN decomposition. Figure 1A shows the time evolution of optical difference spectra for the Soret region upon reacting 5 μM Fe^{III}Mb with 25 μM PN at 12 °C. A spectral transient of an intermediate (**I**) was observed to arise within 3 s with increased absorbance at 422 nm, followed by its slower decay to Fe^{III}Mb (λ_{max}= 409 nm) over the following 25 s (Figure 1A, inset). The absorbance at 409 nm showed a concomitant decrease in the absorbance in the first 3 s followed by a modest increase (Figure 1A, inset). An isosbestic point at 417 nm was maintained over the course of the reaction. Difference spectra were also obtained for the characteristic Q-band region by examining the reaction between 50 μM metMb and 1.5 mM PN at 25 °C. As shown in Figure 1B, distinct absorbance changes were observed

at 503, ~570 and ~590 nm. All these peaks and valleys in the difference spectra corresponded well with the wavelengths for which metMb and ferrylMb have the largest difference in extinction coefficients. Furthermore, the observed isosbestic points in the difference spectra, including 417 nm and 524 nm were also seen when comparing the absorbance spectra of authentic ferrylMb with metMb.[42] Control experiments were performed accordingly with metMb and decomposed PN (that still contained small amounts of H_2O_2) under the above conditions. No rapidly-formed intermediate was observed.

To confirm the identity of the intermediate **I**, double-mixing stopped-flow experiments were carried out by first mixing 20 μM Mb and 100 μM PN for 3 s followed by addition of ascorbate under pseudo-first-order conditions. The decay rate of **I** was found to accelerate from 0.093 s^{-1} to 0.132 s^{-1} with the addition of 9 mM ascorbate as shown in Figure 2. In separate experiments at 12 °C and pH 7.3, ferrylMb was prepared independently by the reaction of metMb (5 μM) and H_2O_2 (100 μM) followed by adding catalase to quench the excess H_2O_2. The reaction rate of authentic ferrylMb with ascorbate was measured to be 4.0 M^{-1} s^{-1} (Figure S1B), consistent both with the reductive trapping of the metMb-PN intermediate described above (4.2 M^{-1} s^{-1}, Figure S1A) and with the literature value, 2.7 ± 0.8 M^{-1} s^{-1}.[43] Hence, intermediate **I** formed during metMb/PN interaction exhibits the same kinetic behavior in reacting with electron donor ascorbate as that of an authentic ferrylMb.

The decay of Mb intermediate **I** back to metMb was studied by following the absorbance changes at 422 nm. The life time of **I** at 12 °C (30 s, Figure 2) is distinctly longer than that of PN (20 s). This behavior indicates that the decay of **I** is mainly (75% ferryl was reduced during 20 s) dependent on its reduction by PN, as well as several other pathways, such as reduction by tyrosine,[42] NO_2^-,[30] nitrite and NO.[44] To clarify the kinetics of this main reduction pathway, ferrylMb was prepared fresh in one syringe by treatment of metMb with H_2O_2 followed by catalase quenching and then rapidly mixed with PN in the other syringe. A first-order treatment in terms of PN could not be applied for the entire process since the concentration of PN was not sufficiently constant at the end of the reaction. Fitting the first 0.5 s decay of ferrylMb at 422 nm to a linear function, the initial rates (v_0) of this bimolecular reaction with different concentrations of PN could be determined. The slope of v_0 vs PN concentration gave a value of (1.53 ± 0.06) × 10^4 M^{-1} s^{-1} at 25 °C (Figure S2A), in good agreement with an earlier report by Herold et al.[45] The rate constant of ferrylMb reduction by PN was measured to be (3.8 ± 0.3) × 10^3 M^{-1} s^{-1} at 12 °C by the same method (Figure S2B). Likewise, the rate constant of nitrite reduction of authentic ferrylMb was measured to be 30 M^{-1} s^{-1} at 25 °C.

MetMb tyrosine is nitrated by peroxynitrite

To achieve an efficient and reproducible mixing of PN with Mb, we used the stopped-flow spectrometer as a mixing device to determine the nitration extents of metMb and cyanide-bound metMb (metMbCN) by PN. We quantified the yields of nitrated metMb by electrospray mass spectrometry (ESI-MS). MetMb, metMbCN and nitrated myoglobin (nitroMb) were found to have equal ionization efficiency by examining standard mixtures. Direct MS detection of the entire reaction mixture avoids errors associated with enzymatic digestion and sample handling when analyzing for the extent of nitration. Reaction of 100 μM metMb with 10 and 30 equiv (1 mM and 3 mM) of PN resulted in 8 ± 1 μM and 10 ± 1 μM mono-nitrated Mb at 25 °C and pH 7.4, respectively, as determined by inspection of the mass spectral data (Figure S3A). The small amounts of Mb nitration observed with decomposed PN solutions were subtracted from the yields observed with active PN (H_2O_2 was < 5% relative to PN concentration). The yields of nitroMb in heme-blocked metMbCN with 1 and 3 mM PN were 21 ± 1 μM and 27 ± 1 μM, respectively. NitroMb was purified by anion exchange HPLC followed by trypsin or Glu-C endoproteinase digestion. The specific nitration site of the nitroMb was identified by LC-MS/MS. In the MS/MS spectra, both Y*LEFISDAIIHVLHSK

from trypsin digestion (Figure S3B) and LKPLAQSHATKHKIPIKY*LE from Glu-C digestion displayed a 45 Da molecular weight increase due to the modification of tyrosine 103, whereas tyrosine 146 was unchanged. These results unambiguously identify Tyr103 as the preferential site of nitration in the PN-mediated horse heart metMb nitration

Fluorescein traps NO_2 evolved from metMb/PN interactions

Fluorescein (Fl) reacts with PN to form two nitrated isomers, 2′- and 4′-nitrofluorescein ($FlNO_2$), the structures of which were confirmed by mass spectrometry and ^{1}H NMR.[46,47] The reaction can be followed conveniently by monitoring the shift of λ_{max} from 490 to 494 nm and the significant absorbance increase at 520 nm ($\varepsilon = 1.13 \times 10^4$ M^{-1} cm^{-1}) (Figure 3). As Fl has negligible absorbance at 520 nm, the total nitration yields of Fl could be determined from the absorbance increase at 520 nm. When mixing 50 μM metMb with 0-50 μM Fl solutions followed by an addition of 30 equiv (1.5 mM) PN at 25 °C, we found that 25 μM Fl entirely suppressed the nitration of 50 μM metMb by 1.5 mM PN.

The mechanism of the metMb/PN interaction was further examined by stopped-flow rapid mixing of metMb, Fl and PN solutions. The experiments were performed by varying the concentration of metMb while keeping the concentrations of Fl and PN constant. Figure 4A shows a representative set of time profiles of PN-mediated $FlNO_2$ formation in the presence of metMb (0, 20 and 50 μM). Control experiments with metMbCN carried out under the same conditions at pH 7.6 showed very little variation in nitroFl yields (data not shown). As seen in Figure 4A (traces a-c in black), addition of 20 and 50μM metMb to Fl reduced the yields of $FlNO_2$ from 26.4 μM to 13.6 and 10.2 μM, respectively. Importantly, the initial $FlNO_2$ formation rates (0-2.5 s) were found to *increase* with added metMb (Figure 4A). Furthermore, the time courses for the formation and decay of the intermediate **I** during the metMb/PN reaction in the presence and absence of Fl were measured at 426 nm at pH 7.4 and 12 °C (Figure 4B). With 10 μM Fl in the medium, the maximum concentration of **I** was noticeably increased.

Numerical simulation validates the radical rebound mechanism in the metMb/PN interaction

Kinetic simulations of intermediate **I** formation and PN-mediated Fl nitration in the presence and absence of metMb were performed with Berkeley-Madonna Modeling and Analysis software. Kinetic modeling was initiated by inputting the reaction equations (eq 1-4 and measured or literature rate constants as shown in Scheme S1). The simulations yielded individual time courses for the concentrations of ferrylMb, NO_2, PN and nitroFl under different conditions. From the simplest model of PN-mediated Fl nitration in the absence of metMb, which is the same as the mechanism of phenol nitration[9] (Scheme S1), we conclude that PN spontaneous decay produced about 10% NO_2. For the simulations of Fl nitration in the presence of various metMb concentrations (Figure 4A), the competition between tyrosine and Fl was explicitly considered (eq 5 and eq 7 in Scheme S1). As Fl proved to be a better trap of NO_2 than the tyrosines in the metMb protein by at least 10 fold, we set the values of tyrosine reactions at one order of magnitude smaller than those for Fl radical reactions ($k_5 > 10\ k_7$). The four core equations as shown below were used to model the effect of metMb on NO_2/$FlNO_2$formation.

$$\mathrm{MbFe^{III}OH_2 + HOONO \xrightarrow[-H^+]{k_{cat}} \left[MbFe^{IV}{=}O \cdot NO_2\right]} \qquad \text{eq 1}$$

$$\left[\mathrm{MbFe^{IV}{=}O \cdot NO_2}\right] \underset{k_e^{-1}}{\overset{k_e(\mathrm{cage-escape})}{\rightleftharpoons}} \mathrm{MbFe^{IV}{=}O + NO_2} \qquad \text{eq 2}$$

$$\left[\mathrm{MbFe^{IV}{=}O \cdot NO_2}\right] \xrightarrow[\mathrm{H_2O}]{\mathrm{k_r(rebound)}} \mathrm{MbFe^{III}OH_2 + NO_3^-} \quad \text{eq 3}$$

$$\mathrm{MbFe^{IV}{=}O + HOONO} \xrightarrow[\mathrm{H^+}]{\mathrm{k_3}} \mathrm{MbFe^{III}OH_2 + NO + O_2} \quad \text{eq 4}$$

The value of k_e^{-1} (1.2×10^7 M^{-1} s^{-1}), representing second-order NO_2 rebinding from solvent, was adopted from the measurements of Goldstein et al.;[30] k_3 ($(1.53 \pm 0.06) \times 10^4$ M^{-1} s^{-1}) was measured by experiment as described above. Since k_e and k_r must be much larger than k_{cat} (the metMb-PN turnover rate: 1.03×10^4 M^{-1} s^{-1} at 25 °C,[14] and k_3 represents only the reduction of cage-escaped ferrylMb (~10% of total Mb). The rate-determining step of this catalytic cycle is the formation of [Fe^{IV}=O ·NO_2]. Hence, the rate constant of the first step ([Fe^{IV}=O ·NO_2] formation via eq 1) is equal to k_{cat}. We found by kinetic simulation that it is the ratio of k_e and k_r that determines the yields of ferrylMb as well as the rates of its generation. The time courses of intermediate ferrylMb formation at 25 °C (Figure 5A) were fit well with k_e/k_r = ~0.1 using the above equations. The observed yields of ferrylMb computed from the known extinction coeffiencts were ~3% of the total Mb with 240 μM PN and ~ 5% of the total Mb with 450 μM PN. As seen in Figure 5A, these yields can also be estimated well by the simulation model described as above.

The rate of intermediate **I** (i.e., ferrylMb) formation as a function of initial PN concentration at constant metMb concentration at pH 7.4 and 25 °C was fit to eq 5 (Figure 5B). With k_r/k_e = 15, the bimolecular rate constant of metMb/PN reaction can be deduced to be 1.0×10^4 M^{-1} s^{-1}. This value matched our measured k_{cat} under these conditions.

$$\frac{\mathrm{d[Fe^{IV}O]_0}}{\mathrm{dt}} = \frac{\mathrm{k_e k_{cat}[Fe^{III}][PN]_0}}{\mathrm{k_e + k_r}} \quad \text{eq 5}$$

The data for reactions between 520 μM PN and 0, 20, 50 μM metMb in the presence of 30 μM Fl as described above were nicely simulated based on equations 1-4 with ~5% trappable NO_2 (Figure 4A, traces a-c in blue, red and green). When simulating the metMbCN-mediated reactions under the same conditions, good fits were achieved by setting k_{cat} to zero, while all other reactions were retained. As shown in Figure 4A, if the cage escape of NO_2 from [ferrylMb ·NO_2] was not considered (k_e=0) in the simulation, the simulated time courses of FlNO_2 formation in the presence of 20 and 50 μM metMb deviated widely from the experimental results (Figure 4A, trace d and e, respectively).

Discussion

The results presented here provide the first direct evidence that the metmyoglobin-peroxynitrite interaction yields ferrylMb ($MbFe^{IV}$=O) concurrently with the formation of freely-diffusing ·NO_2. The data indicate a mechanism that involves rate limiting O-O bond homolysis in a peroxynitrito-Fe^{III}-heme species ($MbFe^{III}$-O-ONO) to afford a caged [Fe^{IV}=O ·NO_2] intermediate (Scheme 1), as we had suggested[14] and in analogy to the process we had earlier delineated for synthetic iron and manganese porphyrins.[34-37] The major pathway to close the catalytic cycle is cage collapse of [Fe^{IV}=O ·NO_2] to form an Fe^{III}-heme and nitrate, a process analogous to ferryl oxygen rebound to carbon radical intermediates.[48] The results also show that ·NO_2 can diffuse away from the heme site to induce nitration elsewhere. To confirm this

latter pathway we employed fluorescein as a chemical trap of $\cdot NO_2$. The yield and kinetics of both ferrylMb formation and $FlNO_2$ formation are used to quantitate the degree of dynamic cage escape of $\cdot NO_2$ into the protein interior and the medium during the catalytic decomposition of PN. Overall, the behavior of NO_2 within the internal Mb cavities is reminiscent of the recombination and escape scenarios observed for photo-dissociated O_2, NO and CO and is further evidence of directed, small molecule processing within the myoglobin structure.[3]

FerrylMb detection and identification

The direct detection of ferrylMb and the kinetics of its formation provide strong evidence for the mechanism of metMb/PN interaction proposed in Scheme 1. Reasonable candidates for the transient intermediate (**I**) include $MbFe^{III}OONO$, $MbFe^{IV}=O$, $MbFe^{III}ONO_2$, $MbFe^{III}NO$, and the nitrito-Fe^{III} adduct,[49] $MbFe^{III}NO_2$. As shown in Figure 1A, the Soret band of metMb shifted from 409 nm to 425 nm for **I** with an isosbestic point at 417 nm. Further, the Q-band absorbance at 503 nm decreased with concurrent increases at 570 nm and 590 nm (Figure 1B). Isosbestic points were apparent at 525 nm and ~ 620 nm. This pattern explicitly excludes the possibility of **I** being $MbFe^{III}OONO$, $MbFe^{III}ONO_2$ or $MbFe^{III}NO_2$, since all of these iron(III) species have Soret maxima below 417 nm,[28] which is the isosbestic point between metMb and **I**.

$MbFe^{III}NO$, which is also a transient species,[50] has a very similar UV-vis absorption spectrum to ferrylMb and intermediate **I** observed here.[51] However, both the absorbance changes in the Q-band region and the kinetic behavior of **I** exclude $MbFe^{III}NO$. Authentic ferrylMb has a broad Q-band centered around 590 nm and an isosbestic point with metMb near 620 nm.[42] In the difference spectrum of authentic 5 μM ferrylMb and metMb maxima are observed at 540 and 588 nm and a zero-crossing (isosbestic) at ~625 nm, similar to what is seen in Figure 1B. By contrast, $MbFe^{III}NO$ has an isosbestic point with metMb at 590 nm.[50] Further, the rate constant for NO dissociation from $MbFe^{III}NO$ has been reported to be very fast, 43 s^{-1} under conditions similar to ours.[50] Given the known rate constant for the PN reaction with metMb, and supposing even 100% efficiency for $MbFe^{III}NO$ formation, that species would not build up significantly and the half-time for decay would be 1 s. Our results show the ferrylMb decay halftime for intermediate I to be 10 s and it persists *after* the completion of PN decay. This is much too slow to be $MbFe^{III}NO$ and is consistent with the known behavior of ferrylMb. Also, the on-rate constant for $[MbFe^{III} + NO \rightarrow MbFe^{III}NO]$ is only 5×10^{-4} $M^{-1}s^{-1}$, a very different situation from the diffusion controlled binding rate of NO to Fe^{II}.[50]

To further differentiate these two possibilities and to identify **I** as ferrylMb and not $MbFe^{III}NO$, we examined the reaction of **I** with ascorbate. Accelerated decay of **I** to $MbFe^{III}$ was observed with increasing concentrations of ascorbate. The reduction of ferrylMb to metMb by ascorbate is reported to have a rate constant of 2.7 M^{-1} s^{-1},[43] while $metMbFe^{III}NO$ is too short-lived to react under such conditions. Significantly, the bimolecular rate constant observed for the reaction of **I** with ascorbate was found to be 4.2 M^{-1} s^{-1} at 12°C and pH 7.4, which matched the measured rate constant between authentic ferrylMb and ascorbate (4.0 M^{-1} s^{-1}) under the same conditions. On this basis we identified intermediate **I** as ferrylMb ($MbFe^{IV}=O$).

We also found that the yield of **I** was enhanced in the presence of fluorescein (Figure 4B) by a small but distinct amount. One can anticipate from Scheme 1 that the efficient capture of NO_2 in the medium by a trapping agent would increase the steady state concentration of $MbFe^{IV}=O$ by decreasing the amount of NO_2 return to the active site ferryl. Taken together, the direct detection of ferrylMb UV-vis absorbances during the metMb/PN reaction, the kinetics of its reduction by ascorbate and the effect of NO_2 trapping described here provide strong evidence for the formation of ferrylMb in the metMb/PN reaction.

Analysis of the kinetics of ferrylMb formation provides a revealing perspective of the metMb/PN reaction. The rate of $MbFe^{IV}=O$ formation was found to be highly dependent on the temperature and PN concentration. To observe ferrylMb, these variables needed to carefully chosen. At 25 °C and with 20 equiv. PN, the peak ferrylMb concentration was achieved within 0.3-1.0 s, while at 12 °C, 4% ferrylMb was formed within 2-3 s with the same amount of PN. Significantly, the overall metMb-PN turnover rate could be well deduced to be 1.0×10^4 M^{-1} s^{-1} from the second-order rate constant for the appearance of ferrylMb. This observation again shows that the detected ferrylMb comes from the PN reaction. The alternate possibility that ferrylMb derives instead from the reaction of the small amounts of hydrogen peroxide in the PN can be excluded because the flux through this reaction would be 400-fold too slow (5% H_2O_2; $k_{H2O2}= 5 \times 10^2$ M^{-1} s^{-1}), [42,52] even in the higher concentration regime used to analyze the changes in the Q-band region. Consistent with this expectation, solutions of decomposed peroxynirite containing the same amount (~5%) of hydrogen peroxide did not show any rapid build-up of **I**.

The spectral transient giving rise to ferrylMb can be treated as an approach to a quasi-steady-state as $\cdot NO_2$ is released from the Mb active site, according to the simplified core catalytic cycle in Scheme 2. The caged radical pair [$Fe^{IV}=O$ $\cdot NO_2$] is not expected to build up to detectable concentrations due to rapid in-cage rebound and cage escape of NO_2 ($k_r \sim k_e \gg k_1$). Similarly, freely-diffusing $\cdot NO_2$ also reaches a low, steady state concentration. The degree of ferrylMb formation depends upon the recombination efficiency with respect to diffusional cage escape of $\cdot NO_2$ (k_e/k_r) and the rate of ferrylMb reduction by PN (k_3).

In its simplest form, the extent and time dependence of ferrylMb build-up in this situation can be understood from Scheme 2, which reflects the balance between the oxidation rate k_1, the fraction of NO_2 cage escape $k_e/(k_e + k_r)$ and the reduction rate, k_3. Kinetic simulations of the measured rates and yields according to Scheme 2 gave $k_e/k_r = 0.10$ (vide infra). We have determined k_3 to be $(1.53 \pm 0.06) \times 10^4$ M^{-1} s^{-1} at 25°C and pH 7.4, which is quite close to the measured k_{obs} and consistent with the original report.[45] FerrylMb can also be reduced by electron transfer from Tyr103[42] and reaction with freely-diffusing NO_2 from the medium by a reencounter mechanism (k_2).[30] The NO_2-mediated ferrylMb reduction produces a Fe^{III}-nitrato complex, which has been found to decompose rapidly to $MbFe^{III}$-OH + NO_3^- with a rate of 190 ± 20 s^{-1}.[30] The reduction of ferrylMb by nitrite is negligible under these conditions ($k = 30$ M^{-1} s^{-1}).

At what point does free $\cdot NO_2$ emerge from the metMb/peroxynitrite interaction? This process can be considered in analogy to geminate recombination of diatomic molecules (NO, O_2 and CO) with deoxy myoglobin. The details of such diffusive cage phenomena within heme proteins have been extensively studied by photophysical techniques that allow the rapid formation of the dissociated heme-ligand intermediate [Mb L] and spectrophotometric monitoring of ligand rebinding (eq 6).[40,41]

$$\mathrm{Mb{-}L} \underset{k_{BA}}{\overset{h\nu}{\rightleftarrows}} [\mathrm{Mb\ L}] \underset{k_{CB}}{\overset{k_{BC}}{\rightleftarrows}} \mathrm{Mb + L_{Xe}} \underset{k_{in}}{\overset{k_{out}}{\rightleftarrows}} \mathrm{Mb + L} \qquad \mathrm{L = CO,\ O_2\ and\ NO} \tag{eq 6}$$

Here, Mb-L is the ligand-bound state, [Mb L] is a caged state with the dissociated ligand (L) located close to the heme iron in the distal pocket while in the Mb + L state the ligand molecule has diffused from the distal pocket into the hydrophobic (xenon) cavities within the protein.[53,54] Small molecules can then diffuse from the Xe cavities into the surrounding medium. This latter process may be conformationally gated since there is no obvious ligand entry/exit pathway in the myoglobin fold.[3] The results have shown that ligand recombination (k_{BA}) in

myoglobin competes with cage escape (k_{BC}), whereby the ligand L diffuses first into the Xe pockets and then into the medium (k_{out}). Typically, the relative efficiency of in-cage ligand capture to cage escape (k_{BA}/k_{BC}) are within an order of magnitude of each other.[40,41] Similar results and conclusions have been reported to describe the behavior of small molecules in solution.[55,56] Ligand recombination in deoxyMb (Fe^{II}) is relatively slow for CO, resulting in diffusive release to the medium after photolysis.[57] By contrast, the NO binding process, which is nearly barrierless, leads to efficient ligand capture by the ferro-heme, while for O_2, rebinding and cage escape occur with similar efficiency in deoxyMb.[41]

The kinetics of NO rebinding to deoxyMb have been shown to be biphasic. This feature of the data has been interpreted to be the result of very rapid NO recombination from the distal pocket within 10 ps and a slower (200 ps) binding process of NO molecules from the Xe cavities.[58] Statistical mechanics simulations have shown that 5% of the NO molecules were still found in the distal pocket and Xe cavities even after 1 ns.[59] The kinetic barrier to this slower recombination phase has been associated with entropic considerations, solvent effects and the dynamics of conformational gating for diffusive return to the distal pocket.[57,58,60]

The results for the reaction of myoglobin with peroxynitrite indicate that this ligand capture and escape scenario applies as well for the behavior of [$MbFe^{IV}$=O ·NO_2] (Figure 6). Here the NO_2 formed at the active site by O-O bond homolysis in the rate-limiting step can react with the ferryl oxygen to form nitrate (k_r) or retreat into the protein interior (k_e). Moreover, Figure 6 illustrates that Tyr103 is preferentially nitrated, as was unambiguously determined from mass spectroscopic peptide sequence analysis on the purified mono-nitroMb. This nitration selectivity is likely caused by better solvent accessibility of this tyrosine as well as its co-planar donor-to-acceptor orientation with the heme.[61] Interestingly, the degree of cage escape of NO_2 observed for the myoglobin reaction is similar to the behavior of *alkyl* peroxynitrites upon rearrangement to alkyl nitrates.[62] In further analogy to this stochastic behavior of incipient radical pairs, we have recently shown that cage escape competes with cage recombination during the C-H bond hydroxylation reaction of the diiron hydroxylase AlkB,[63] suggesting that this phenomenon may be more general in metalloenzyme catalysis.

Fluorescein as a probe of NO_2 cage escape

The observed nitration of fluorescein by peroxynitrite in the presence of metMb confirmed the release of freely diffusing NO_2 from the protein during PN turnover. The signature spectral changes accompanying $FlNO_2$ formation allowed both a convenient assay of NO_2 produced and a sensitive measure of the rate of its evolution (Figure 3). The data showing the overall yield of $FlNO_2$ and the time course of its production in the presence of metMb (Figure 4A) show distinctly *faster* Fl nitration with 50 μM metMb than was observed with 20 μM metMb. Further, the decrease in $FlNO_2$ yield upon doubling the metMb concentration was only 20%. The presence of equal amounts of Fl in the medium completely suppressed protein tyrosine nitration. This observation shows that Fl is at least a 10-fold more efficient trap of NO_2 than tyrosine within Mb. Further, protection of tyrosine by Fl shows that both probes are sampling the same pool of NO_2. The increase in the amount of ferrylMb detected during PN decay in the presence of Fl, noted above, is a further confirmation that freely diffusing NO_2 is present in the system, some of which re-encounters ferrylMb at the active site. PN spontaneous decay produced about 10% $FlNO_2$, which is consistent with the measurements of available NO_2 from PN decay reported by Ingold.[64] By comparison, the yields of $FlNO_2$ indicated about 5% trappable NO_2 from the Mb-mediated route. This value is in qualitative agreement with the 10% efficiency of NO_2 cage escape derived from the ferrylMb kinetics but less than the 20% estimate described in our initial study.[14] The fact that fluorescein nitration detects only half of the total NO_2 produced is suggestive of the amount of NO_2 in the xenon cavities[58,59] that

returns to react with ferrylMb without diffusing into the medium. It is also clear from these results that myoglobin reduces the net amount of trappable NO_2 by only a factor of two.

The unambiguous observation of the ferrylMb intermediate provides strong confirmation of the proposed mechanism, in which the transient intermediate [Fe^{IV}=O ·NO_2] can either proceed to cage escape or rebound to form nitrate and ferric Mb. The decomposition of PN catalyzed by water soluble iron(III) porphyrins (e.g., FeTMPS and FeTMPyP) affords significant amounts of oxoFe^{IV} porphyrins.[34,35] In particular, the fast rebound of NO_2 to Fe^{IV}TMPS accounts for an important pathway for oxoFe^{IV} reduction to Fe^{III}. The rate constant of this rebound can be as fast as 1.7×10^7 M^{-1} s^{-1},[34] which is the same as the experimental result obtained by Goldstein et al. with ferrylMb and NO_2 (1.2×10^7 M^{-1} s^{-1}).[30]

Kinetic simulation of the peroxynitrite-myoglobin reaction

Since all of the pertinent rate constants for spontaneous and Mb-catalyzed PN decay are known, it was possible to explicitly simulate the reaction mechanism discussed above (Scheme 2) and the effect of added fluorescein. The enhanced initial rate of $FlNO_2$ formation, the crossing of the yield curves at 2.5 s and the degree of product yield decrease with increasing [metMb] were all reproduced very closely by the kinetic simulation (Figure 4A, traces a-c). The observed amount of ferrylMb under turnover conditions required 10% escape of NO_2 from the distal pocket ($k_e/k_r = 0.1$), while the kinetics and yield of $FlNO_2$ led to a best fit with 5% NO_2 escape into the medium. By contrast, the experimental data for Fl nitration (Figure 4A traces a-c in black) was completely inconsistent with the simulation (Figure 4A, traces d and e) if k_e was not included. The data showed 60-100% more $FlNO_2$ observed experimentally than predicted if there was no cage escape of NO_2. The simulation also allowed an estimation of the formation and decay of NO_2 through the various reaction channels. The generation of NO_2 results mainly from PN spontaneous decomposition and cage escape. In a metMb/PN (1:30) reaction, NO_2 is consumed predominantly by dimerization and hydrolysis (50%), reencounter with the ferrylMb (k_2) to form nitrate (k_r) (30%) and tyrosine nitration (20%).

The results illuminated here for the reaction of PN with metMb are pertinent to the discussion regarding the roles of oxyMb and oxyHb in trapping NO *in vivo*,[31,65] since the two processes intersect at the Fe(III)-OONO intermediate. Recently, this *NO dioxygenase* activity has been extended to other myoglobin-like proteins, such as neuroglobin,[66] cytoglobin[65] and bacterial hemoglobins.[67] One would expect, *a priori*, that ferrylMb and NO_2 would be formed to the same extent from the oxyMb/NO reaction as from metMb and PN. Olson and Gardner have recently described a careful analysis of the isotopic content of nitrate resulting from the reaction of $^{18}O_2$-oxyMb with NO.[32] The results showed 99% dioxygenation of NO to afford $^{18}O_2$-^{16}O-nitrate via rebound to ferrylMb. Significantly, when we simulated the fate of ferrylMb and NO_2 formed from the single-turn-over reaction of $^{18}O_2$-oxyMb with NO using the same kinetic scheme described above (Scheme 2) and the known rate constant for oxyMb + NO,[28] we also find only ~1% singly labeled nitrate, quantitatively consistent with the experimental result. The cage recombination mechanism affords little singly-labeled nitrate in the oxyMb/NO reaction because the concentration of NO_2 is low under these conditions, making the bimolecular dimerization-hydrolysis pathway inefficient compared to NO_2 rebound and tyrosine nitration.

Interestingly, computational studies of the NO reaction with oxyMb by Siegbahn[68] and the truncated hemoglobin (HbN) by Crespo[69] also find step-wise processes involving a caged [Fe^{IV}=O ·NO_2] intermediate analogous to Scheme 2. The free energy barrier to O-O bond cleavage in the Fe^{III}-O-ONO intermediate for myoglobin was found to be only 5.2 kcal/mol and formation of the [Fe^{IV}=O ·NO_2] intermediate was exergonic by 6.6-11.2 kcal/mol, with the range depending on the entropy considerations. Oxygen rebound to form nitrate was found to be highly exergonic (-24.7 kcal/mol) with a negligible enthalpic barrier to capture of NO_2

by Fe^{IV}=O. The computed free energy barrier to this NO_2 rebound was found to lie between 2.7 and 7.2 kcal/mol depending on how the entropy of NO_2 was treated. Overall, the experimental results for the metMb PN reaction described here are in remarkable agreement with the calculated reaction energy landscape. The detection of ferrylMb and freely diffusing NO_2 suggests that the larger of the calculated exothermicities for NO_2 formation and the larger of the entropy barriers, both resulting from the more loosely bound NO_2, are closer to the real situation.

Conclusions

The reaction of metMb with PN has been shown by direct detection to afford a ferrylMb intermediate and freely-diffusing NO_2. This mechanism is similar overall to the reaction of PN with water-soluble iron porphyrins. Rapid O-O bond homolysis of an intermediate peroxynitrito-Fe^{III} complex affords a caged [Fe^{IV}=O $\cdot NO_2$] ensemble from which $\cdot NO_2$ may either rebound to form nitrate (90%) or escape the cage (5-10%) to nitrate tyrosine or other targets such as added Fl. The amounts of NO_2 and free ferrylMb liberated from this radical cage are dependent on the internal structure and gating dynamics of the protein in a manner similar to cage recombination of NO to the Fe(II) heme. The less obvious ferryl intermediate in the horse heart metMb/PN interaction compared with the ones observed from the synthetic porphyrins FeTMPS, FeTMPyP or myeloperoxidase reactions, can be attributed to its compact heme cavity and peptide structure. Overall, the results show that the protein fold of myoglobin modifies the fates of the ferryl and NO_2 intermediates that would derive from nitric oxide scavenging *in vivo*, nonetheless, freely diffusing NO_2 does emerge from this encounter in amounts similar to that of spontaneous PN decay.

Experimental Procedures

Reagents

Horse heart myoglobin, catalase, potassium ferricyanide, sodium nitrite, sodium nitrate, sodium hydroxide, fluorescein and L-ascorbic acid were purchased from Sigma. Hydrogen peroxide (30%) and perchloric acid (70%) were obtained from J.T. Baker. Diethylenetriamine-pentaacetic acid (DTPA) was obtained from Alfa Aesar. Peroxynitrite was synthesized from hydrogen peroxide and nitrous acid as described [70,71] using a sp250i syringe pump (KD scientific). To avoid any contamination with bicarbonate from ambient air, all reagents for peroxynitrite synthesis were degassed with argon thoroughly before using. Synthesized peroxynitrite was collected and kept under argon. Contaminating hydrogen peroxide was reduced to less than 5% (molar ratio) of peroxynitrite by manganese dioxide treatment. Peroxynitrite concentrations were determined at 302 nm (ε_{302} = 1670 M^{-1} cm^{-1}).[72] Except where noted otherwise, PN solutions were 1 mM or less to minimized second-order decay.[73] Peroxynitrite solutions were prepared by diluting the stock solution immediately before use with 0.01 M NaOH to achieve the required concentrations. All the solutions involving the reactions with peroxynitrite were purged with argon vigorously before mixing.

After dissolving myoglobin (horse heart, Sigma) in 0.1 M (pH 7.2) phosphate buffer, a small amount of potassium ferricyanide was added to oxidize the possible remaining oxyMb in solution. The protein was then purified chromatographically over an Econo-Pac 10DG column (Bio-Rad). The concentration of metMb was determined by measuring the absorbance at 409 nm (ε_{408} = 188 mM^{-1} cm^{-1}).[74] The cyanide-bound form of metMb (metMbCN) was prepared by adding a small excess of KCN to the metMb stock solution. The concentrations of metMbCN solutions were determined by measuring the absorbance at 422 nm (ε_{422} = 116 mM^{-1} cm^{-1}).[74] UV/Vis spectra were obtained on a HP 8452A diode array spectrometer. All UV/Vis spectra were recorded at room temperature.

Stopped-Flow Kinetic Analysis and metMb nitration by PN

Stopped-flow kinetic studies were carried out using a Hi-Tech SF-61DX2 double mixing stopped-flow spectrophotometer (Hi-Tech, Salisbury, UK). The reactions were monitored either at a selected wavelength (single wavelength mode) or by using a diode array detector to record the entire visible range at each time point. For all the studies of the reactions under CO_2-free conditions, the stopped-flow lines were washed with argon-purged doubly deionized water immediately before the experiments. Thoroughly degassed solutions of metMb, PN and other reactants were transferred in Hamilton gastight syringes right before mixing. Several shots were collected as fast as possible. With all these efforts, essentially no CO_2 was involved during the mixing of fluorescein/metMb and PN. The traces were averaged from at least three shots. Kinetic data was analyzed and fitted on KinetAsyst software provided by Hi-Tech. The nitrated Mb solutions were collected at the outlet of the stopped-flow. When Mb samples were treated with PN in the presence of fluorescein, proteins were separated from fluorescein by Microcon YM-3 (MWCO 3000) centrifugal filter devices (Millipore) and subsequently recovered prior to MS determination.

To confirm the identity of intermediate I, double mixing stopped-flow experiments were carried out to study its decomposition process in the absence and presence of ascorbate. In the first mixing, 20 μM metMb in syringe A was mixed with an equal volume of 100 μM PN in syringe B. The reaction mixture was aged for 3 s to allow the full development of intermediate I (Intermediate I was observed to reach its maximum around 2.5s under the same conditions). The products of the first mixing were subsequently mixed with an equal volume of ascorbate solution from syringe C. The double mixing experiments were studied at wavelengths 422 nm, 409 nm and 302 nm.

Calculations and data treatment were performed using Microsoft Excel and a commercial graphics and data analysis software (OriginPro 7.5, OriginLab).

HPLC-MS analysis

Nitrated protein mixtures were thoroughly dialyzed (Slide-A-Lyzer mini Dialysis units, 7,000 MWCO, Pierce) against water prior to further analysis by an Agilent 6510 LC Q-TOF MS. This Q-TOF was coupled with an Agilent HPLC-chip (G4240-62001, Zorbax 300SB-C18) for sample loading and separation. The proteins were eluted over a course of 15 min by using a nonlinear gradient of 3% to 90% acetonitrile containing 0.1% formic acid at a flow rate of 0.5 μL/min. Proteins eluted from HPLC-chip were directly injected into the coupled Q-TOF MS. MS data were acquired and processed using Agilent MassHunter workstation and included analysis software. LC/MS analysis of fluorescein and its nitrated products was performed with an Agilent MSD apparatus with a UV/Vis detector, equipped with a Mercury MS (phenomenex) column (20 × 2.0 mm).

NanoLC-MS/MS analysis

Nitrated Mb was purified using anion exchange semi-preparative HPLC (column: PL-SAX, 1000Å, 8 μM 150 × 7.5mm, Polymer Laboratories). Solvent A is 20 mM Tris-$HClO_4$ (pH 8.0), and solvent B is 20mM Tris-$HClO_4$/0.5M NaCl (pH 8.0). Nitrated Mb and native Mb were eluted using an increasing linear gradient of solvent B from 0-80 % in 35 min with a flow rate of 0.8 mL/min. The 409 nm-active fractions were collected and identified by MS. Purified mono-nitrated myoglobin was digested overnight at 37 °C with modified trypsin (Promega, Madison, WI) or GluC endoproteinase (Roche, Germany) in NH_4HCO_3 buffer (50 mM, pH 8). A fused-silica capillary nano-column packed with reverse phase Eclipse XDB-C18 packing materials was employed to separate digested peptides. Peptides were eluted over the course of 150 min by using a nonlinear gradient of 5% to 80% acetonitrile containing 0.1% formic acid, at a flow rate of 120 nL/min. Tandem mass spectra were collected by an LCQ DECA XP PLUS

mass spectrometer controlled by Xcalibur software (ThermoFisher). The acquired MS/MS spectra were automatically searched against a protein database for horse heart myoglobin using SEQUEST algorithm to identify the nitrotyrosine-containing peptides.

Computer Simulations

Kinetic simulations were performed with Berkeley Madonna Modeling and Analysis of Dynamic Systems software, version 8.3.22. (http://www.berkeleymadonna.com).

Supplementary Material

Refer to Web version on PubMed Central for supplementary material.

Acknowledgments

We are grateful for support of this research by the National Institutes of Health (2R37 GM036298).

References

1. Wittenberg BA, Wittenberg JB. Annu Rev Physiol 1989;51:857–78. [PubMed: 2653210]
2. Brunori M. Trends in Biochem Sci 2001;26:209–210. [PubMed: 11295538]
3. Frauenfelder H, McMahon BH, Austin RH, Chu K, Groves JT. Proc Natl Acad Sci U S A 2001;98:2370–4. [PubMed: 11226246]
4. Hendgen-Cotta UB, Merx MW, Shiva S, Schmitz J, Becher S, Klare JP, Steinhoff HJ, Goedecke A, Schrader J, Gladwin MT, Kelm M, Rassaf T. Proc Natl Acad Sci U S A 2008;105:10256–10261. [PubMed: 18632562]
5. Cossins A, Berenbrink M. Nature 2008;454:416–417. [PubMed: 18650904]
6. Pacher PA, Beckman JS, Liaudet L. Physiol Rev 2007;87:315–424. [PubMed: 17237348]
7. Fraser J, de Mello LV, Ward D, Rees HH, Williams DR, Fang YC, Brass A, Gracey AY, Cossins AR. Proc Natl Acad Sci U S A 2006;103:2977–2981. [PubMed: 16469844]
8. Beckman JS, Beckman TW, Chen J, Marshall PA, Freeman BA. Proc Natl Acad Sci U S A 1990;87:1620–1624. [PubMed: 2154753]
9. Goldstein S, Merenyi G. Method Enzymol 2008;436:49–61.
10. Marla SS, Lee J, Groves JT. Proc Natl Acad Sci U S A 1997;94:14243–8. [PubMed: 9405597]
11. Denicola A, Souza JM, Radi R. Proc Natl Acad Sci U S A 1998;95:3566–71. [PubMed: 9520406]
12. Szabo C, Ischiropoulos H, Radi R. Nat Rev Drug Discov 2007;6:662–680. [PubMed: 17667957]
13. Groves JT. Curr Opin Chem Biol 1999;3:226–35. [PubMed: 10226050]
14. Bourassa JL, Ives EP, Marqueling AL, Shimanovich R, Groves JT. J Am Chem Soc 2001;123:5142–3. [PubMed: 11457363]
15. Herold S, Matsui T, Watanabe Y. J Am Chem Soc 2001;123:4085–6. [PubMed: 11457162]
16. Herold S, Shivashankar K. Biochemistry 2003;42:14036–46. [PubMed: 14636072]
17. Pietraforte D, Salzano AM, Scorza G, Marino G, Minetti M. Biochemistry 2001;40:15300–9. [PubMed: 11735412]
18. Gebicka L, Didik J. J Inorg Biochem 2007;101:159–164. [PubMed: 17056120]
19. Floris R, Piersma SR, Yang G, Jones P, Wever R. Eur J Biochem 1993;215:767–775. [PubMed: 8394811]
20. Furtmuller PG, Jantschko W, Zederbauer M, Schwanninger M, Jakopitsch C, Herold S, Koppenol WH, Obinger C. Biochem Bioph Res Co 2005;337:944–954.
21. Batthyany C, Souza JM, Duran R, Cassina A, Cervenansky C, Radi R. Biochemistry 2005;44:8038–8046. [PubMed: 15924423]
22. Cassina AM, Hodara R, Souza JM, Thomson L, Castro L, Ischiropoulos H, Freeman BA, Radi R. J Biol Chem 2000;275:21409–21415. [PubMed: 10770952]

23. Marechal A, Mattioli TA, Stuehr DJ, Santolini J. J Biol Chem 2007;282:14101–14112. [PubMed: 17369257]
24. Daiber A, Herold S, Schoneich C, Namgaladze D, Peterson JA, Ullrich V. Eur J Biochem 2000;267:6729–6739. [PubMed: 11082183]
25. Herold S, Fago A, Weber RE, Dewilde S, Moens L. J Biol Chem 2004;279:22841–22847. [PubMed: 15020597]
26. Herold S, Kalinga S, Matsui T, Watanabe Y. J Am Chem Soc 2004;126:6945–55. [PubMed: 15174864]
27. Herold S, Shivashankar K, Mehl M. Biochemistry 2002;41:13460–72. [PubMed: 12416992]
28. Herold S, Exner M, Nauser T. Biochemistry 2001;40:3385–95. [PubMed: 11258960]
29. Doyle MP, Hoekstra JW. J Inorg Biochem 1981;14:351–358. [PubMed: 7276933]
30. Goldstein S, Merenyi G, Samuni A. J Am Chem Soc 2004;126:15694–701. [PubMed: 15571391]
31. Olson JS, Foley EW, Rogge C, Tsai AL, Doyle MP, Lemon DD. Free Radical Biol Med 2004;36:685–697. [PubMed: 14990349]
32. Gardner PR, Gardner AM, Brashear WT, Suzuki T, Hvitved AN, Setchell KDR, Olson JS. J Inorg Biochem 2006;100:542–550. [PubMed: 16439024]
33. Groves JT, Marla SS. J Am Chem Soc 1995;117:9578–9579.
34. Shimanovich R, Groves JT. Arch Biochem Biophys 2001;387:307–17. [PubMed: 11370855]
35. Lee JB, Hunt JA, Groves JT. J Am Chem Soc 1998;120:7493–7501.
36. Lee JB, Hunt JA, Groves JT. J Am Chem Soc 1998;120:6053–6061.
37. Shimanovich R, Hannah S, Lynch V, Gerasimchuk N, Mody TD, Magda D, Sessler J, Groves JT. J Am Chem Soc 2001;123:3613–4. [PubMed: 11472141]
38. Stern MK, Jensen MP, Kramer K. J Am Chem Soc 1996;118:8735–8736.
39. Sheng X, Horner JH, Newcomb M. J Am Chem Soc 2008;130:13310–13320. [PubMed: 18788736]
40. Austin RH, Beeson KW, Eisenstein L, Frauenfelder H, Gunsalus IC. Biochemistry 1975;14:5355–5373. [PubMed: 1191643]
41. Jongeward KA, Magde D, Taube DJ, Marsters JC, Traylor TG, Sharma VS. J Am Chem Soc 1988;110:380–387.
42. Lardinois OM, Ortiz de Montellano PR. Biochemistry 2004;43:4601–4610. [PubMed: 15078107]
43. KrogerOhlsen M, Skibsted LH. J Agr Food Chem 1997;45:668–676.
44. Herold S, Rehmann FJ. J Biol Inorg Chem 2001;6:543–55. [PubMed: 11472018]
45. Exner M, Herold S. Chem Res Toxicol 2000;13:287–93. [PubMed: 10775329]
46. Shimanovich, R. PhD Thesis, Princeton University. 2003.
47. Jiang Q, Hurst JK. J Biol Chem 1997;272:32767–72. [PubMed: 9407050]
48. Groves JT. Proc Natl Acad Sci U S A 2003;100:3569–74. [PubMed: 12655056]
49. Copeland DM, SoareS AS, West AH, Richter-Addo GB. J Inorg Biochem 2006;100:1413–1425. [PubMed: 16777231]
50. Laverman LE, Wanat A, Oszajca J, Stochel G, Ford PC, van Eldik R. J Am Chem Soc 2001;123:285–93. [PubMed: 11456515]
51. Behan RK, Hoffart LM, Stone KL, Krebs C, Green MT. J Am Chem Soc 2007;129:5855–5859. [PubMed: 17432853]
52. Matsui T, Ozaki S, Liong E, Phillips GN Jr, Watanabe Y. J Biol Chem 1999;274:2838–44. [PubMed: 9915818]
53. Olson JS, Phillips GN. J Biol Chem 1996;271:17593–17596. [PubMed: 8698688]
54. Schoenborn BP, Watson HC, Kendrew JC. Nature 1965;207:28. [PubMed: 5893727]
55. Oelkers AB, Scatena LF, Tyler DR. J Phys Chem A 2007;111:5353–5360. [PubMed: 17552498]
56. Oelkers AB, Tyler DR. Photochem Photobiol Sci 2008;7:1386–1390. [PubMed: 18958326]
57. Goldbeck RA, Bhaskaran S, Ortega C, Mendoza JL, Olson JS, Soman J, Kliger DS, Esquerra RM. Proc Natl Acad Sci U S A 2006;103:1254–1259. [PubMed: 16432219]
58. Ionascu D, Gruia F, Ye X, Yu A, Rosca F, Beck C, Demidov A, Olson JS, Champion PM. J Am Chem Soc 2005;127:16921–16934. [PubMed: 16316238]

59. Nutt DR, Meuwly M. Biophys J 2006;90:1191–1201. [PubMed: 16326913]
60. Frauenfelder H, McMahon BH, Fenimore PW. Proc Natl Acad Sci U S A 2003;100:8615–8617. [PubMed: 12861080]
61. Makinen MW, Schichman SA, Hill SC, Gray HB. Science 1983;222:929–931. [PubMed: 6415814]
62. Goldstein S, Lind J, Merenyi G. J Phys Chem A 2004;108:1719–1725.
63. Austin RN, Luddy K, Erickson K, Pender-Cudlip M, Bertrand E, Deng D, Buzdygon RS, van Beilen JB, Groves JT. Angew Chem Intl Edit 2008;47:5232–5234.
64. Richeson CE, Mulder P, Bowry VW, Ingold KU. J Am Chem Soc 1998;120:7211–7219.
65. Mammen PP, White J, McGrath AJ, Kanatous SB, Horton JW, Garry DJ. Circulation 2003;108:291–291.
66. Brunori M, Giuffre A, Nienhaus K, Nienhaus GU, Scandurra FM, Vallone B. Proc Natl Acad Sci U S A 2005;102:8483–8488. [PubMed: 15932948]
67. Ascenzi P, Bocedi A, Bolognesi M, Fabozzi G, Milani M, Visca P. Biochem Bioph Res Co 2006;339:450–456.
68. Blomberg LM, Blomberg MRA, Siegbahn PEM. J Biol Inorg Chem 2004;9:923–935. [PubMed: 15452775]
69. Crespo A, Marti MA, Kalko SG, Morreale A, Orozco M, Gelpi JL, Luque FJ, Estrin DA. J Am Chem Soc 2005;127:4433–4444. [PubMed: 15783226]
70. Saha A, Goldstein S, Cabelli D, Czapski G. Free Radical Biol Med 1998;24:653–9. [PubMed: 9559878]
71. Uppu RM, Squadrito GL, Cueto R, Pryor WA. Method Enzymol 1996;269:285–96.
72. Koppenol WH, Kissner R, Beckman JS. Methods Enzymol 1996;269:296–302. [PubMed: 8791658]
73. Kissner R, Koppenol WH. J Am Chem Soc 2002;124:234–239. [PubMed: 11782175]
74. Rossifanelli A, Antonini E, Caputo A. Adv Protein Chem 1964;19:73–222. [PubMed: 14268787]

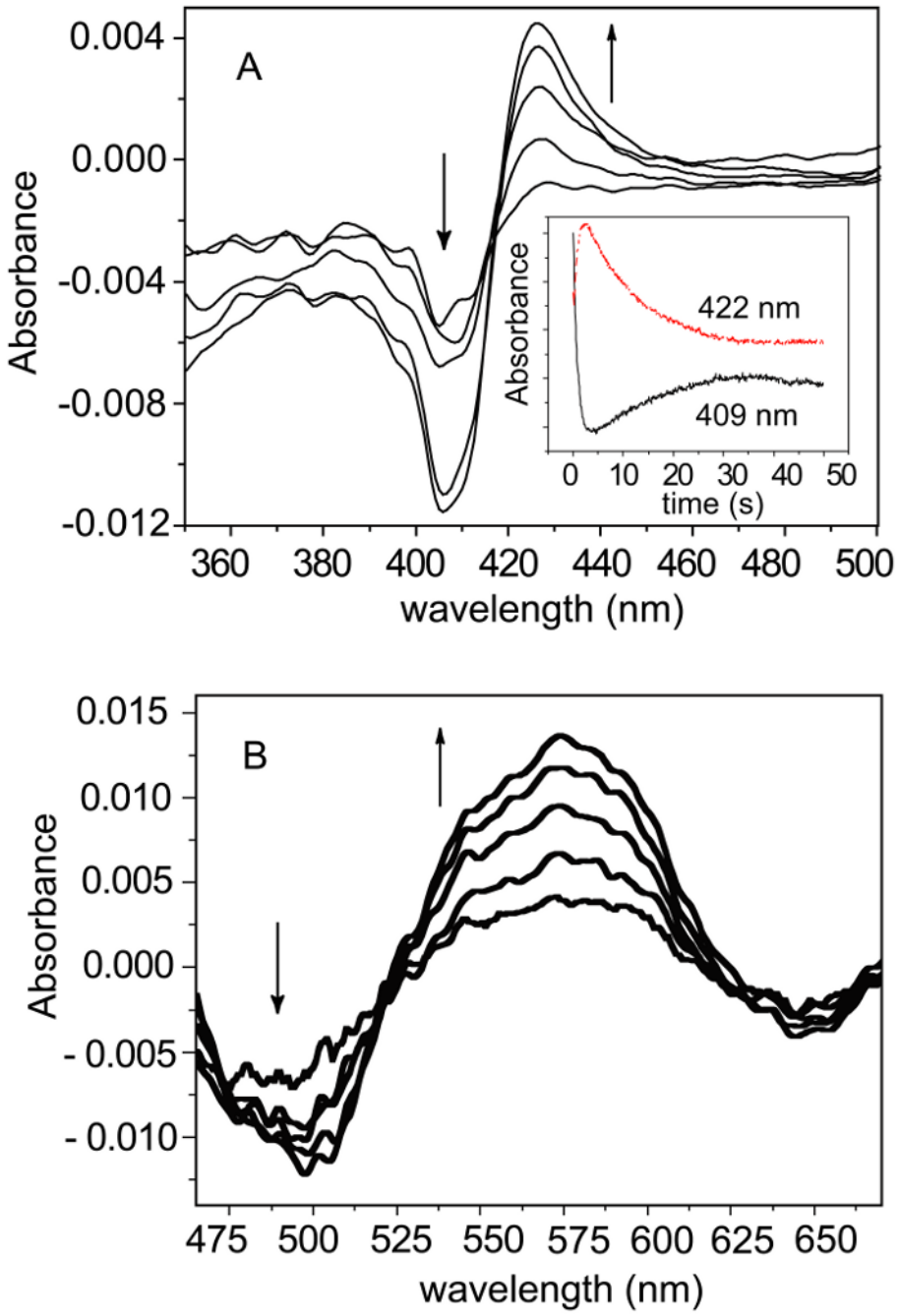

Figure 1.

Formation of intermediate **I** from metMb and PN reaction. (A). Soret absorption difference spectra obtained from the reaction of 5 μM metMb and 25 μM PN at pH 7.4 and 12 °C. The transients were obtained by subtracting the mixture spectrum at 0.02 s from those at 0.2, 0.5, 1, 2 and 3 s. Inset: time courses of the reaction at 422 and 409 nm under above conditions (B). Q-band absorption difference spectra obtained from the reaction of 50 μM metMb and 1.5 mM PN at pH 7.4 and 25 °C. The difference spectra were obtained by subtracting the mixture spectrum at 0.01 s from those at 0.03, 0.06, 0.12 and 0.2 and 0.3 s.

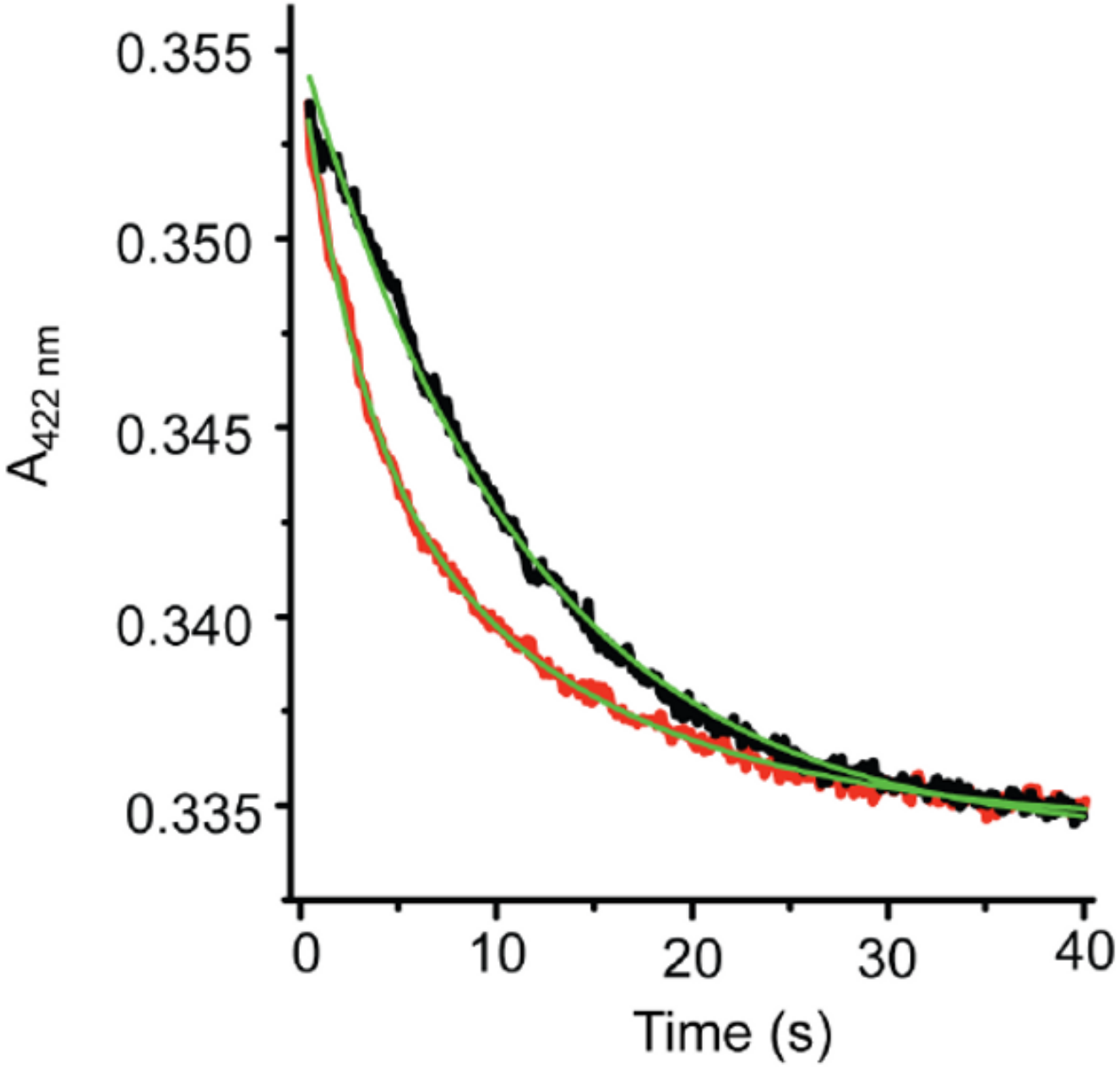

Figure 2.

Decay of intermediate **I** in the absence and presence of 9 mM ascorbate monitored at 422 nm. The experiments were carried out in a double-mixing stopped-flow spectrometer by first mixing 20 μM Mb and 100 μM PN for 3 s followed by addition of buffer (black trace) or ascorbate solution (red trace) under pseudo-first-order conditions at pH 7.4 and 12 °C. First exponential decay equations were used to fit the experimental curves. The values of k_{obs} from those two fittings (green) are 0.093 s^{-1} (black) and 0.132 s^{-1} (red), respectively.

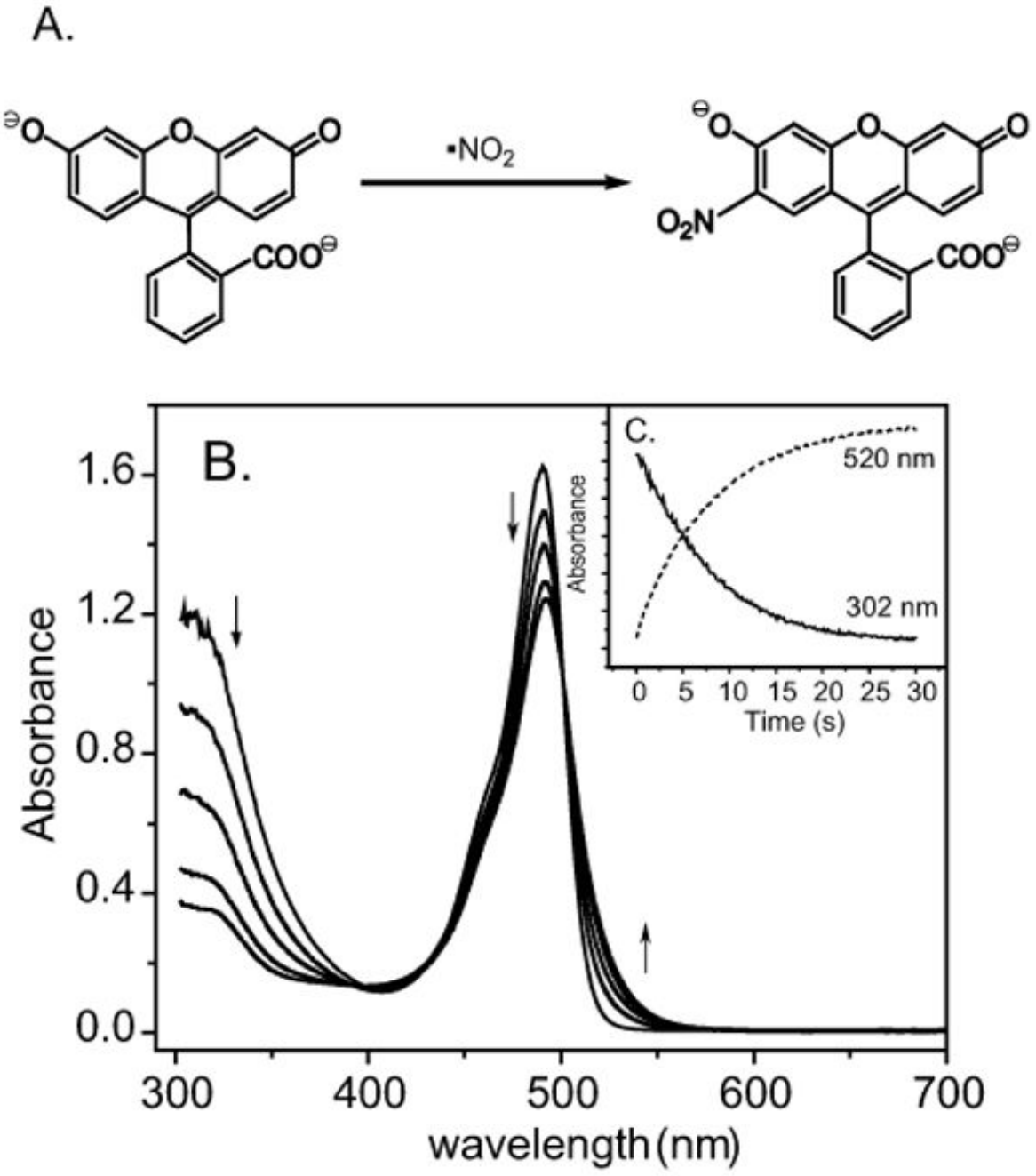

Figure 3.

Nitration of fluorescein by PN. (A). Interaction of Fl and PN produces nitroFl. (B). Stopped-flow rapid-scan UV-Vis spectra of the reaction between 15 μM Fl and 800 μM PN in 0.1 M phosphate buffer at pH 7.4 and 25 °C. Traces shown were taken at 0, 2, 5, 10 and 15 s. The directions of spectral changes are indicated by arrows. (C) The traces exhibit PN decomposition (302 nm, solid line) and, concurrently, nitroFl formation (520 nm, dash line) observed by stopped-flow spectrophotometry upon mixing equal volumes of 50 μM fluorescein with 920 μM peroxynitrite at pH 7.4 and 25 °C.

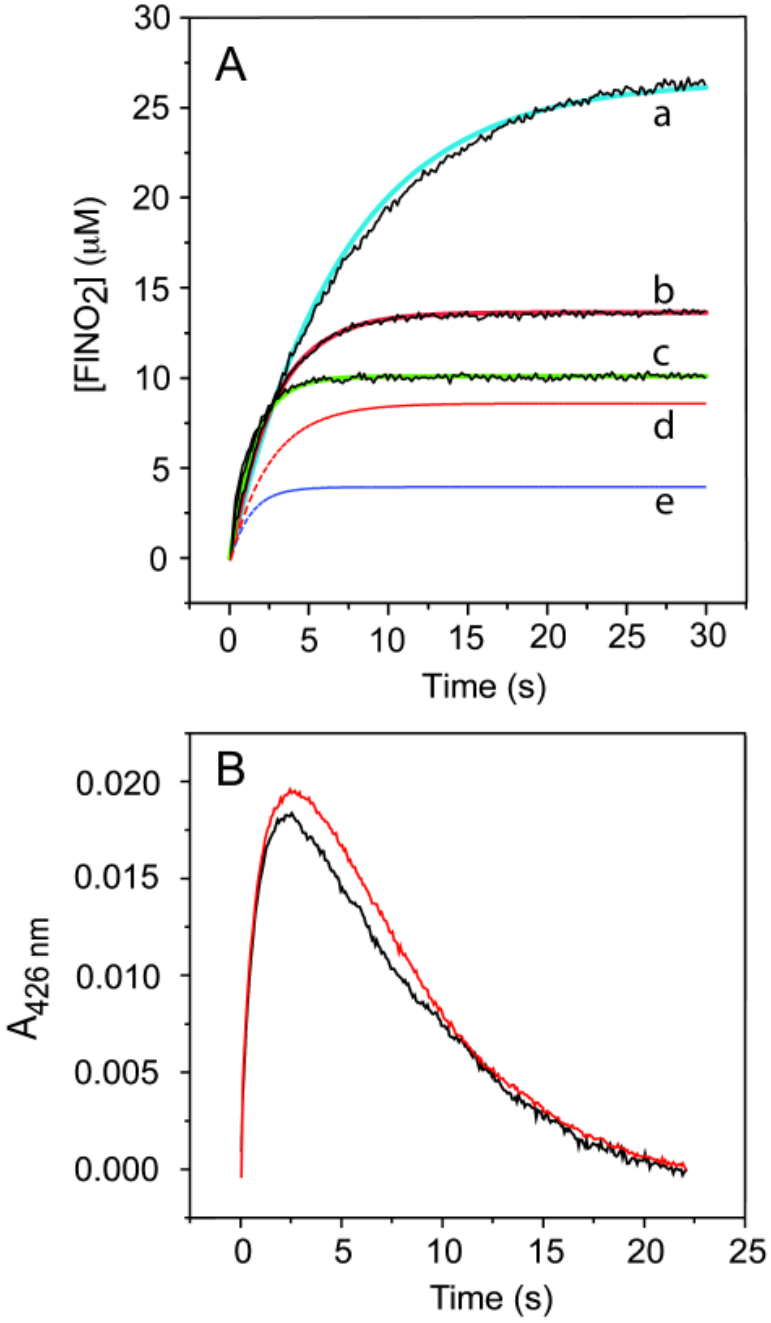

Figure 4.

(A) Overlay of the experimental and simulated time courses of nitroFl formation in the presence and absence of metMb. The parameters were set as shown in eq 1-4 and Scheme S1. Experiments (E) and simulations (S) were done under the same reaction conditions: 30 μM Fl, 520 μM PN, 0, 20 and 50 μM metMb. From top to bottom: 0 μM metMb (a, E in black and S in blue), 20 μM metMb (b, E in black and S in red), 50 μM metMb (c, E in black and S in green), 20 μM metMb with $k_e = 0\ s^{-1}$ (d, S in dash line and red) and 50 μM metMb with $k_e = 0\ s^{-1}$ (e, S in dash line and blue). (B) The formation and decay of intermediate **I** during the reaction of 10 μM (final concentration) metMb and 100 μM PN in the absence (black) and presence (red) of 10 μM Fl at pH 7.4 and 12 °C.

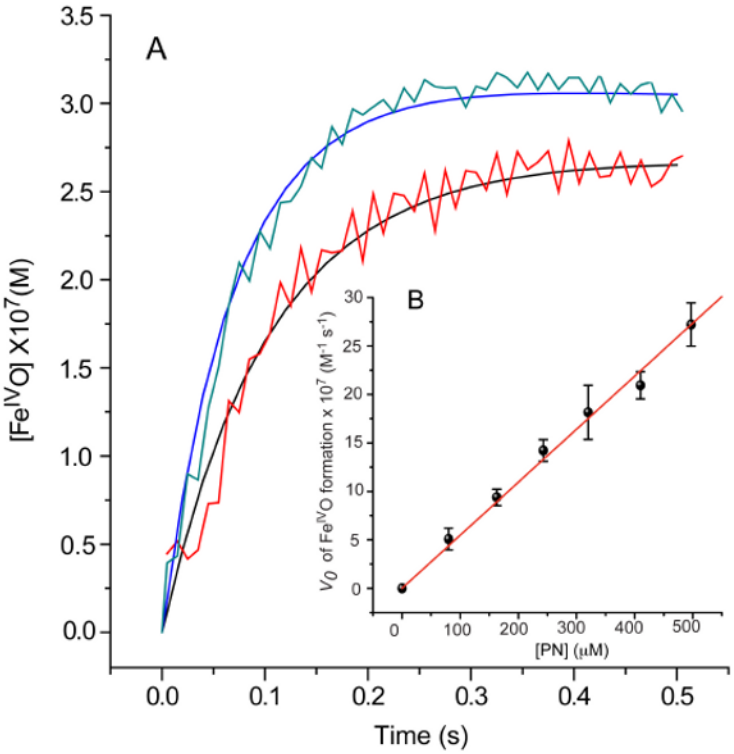

Figure 5.

(A) Experimental and simulated time courses of intermediate ferrylMb formation at pH 7.4 and 25 °C. Reaction conditions: 8.4 μM metMb with 450 μM PN (experimental trace in blue, simulated in black) or with 240 μM PN (experimental trace in red, simulated in black). The parameters used are: k_{cat}=1.0 × 10^4 M^{-1} s^{-1}, k_3= 1.53 × 10^{4}M^{-1} s^{-1} and k_e/k_r=1/10. Tyrosine nitration was not considered in this set of simulations. (B) Plot of intermediate **I** initial formation rates observed at 422 nm vs initial PN concentrations. The reactions were conducted by mixing 8.4 μM metMb with various concentrations of PN in the stopped-flow spectrophotometer at pH 7.4 and 25 °C.

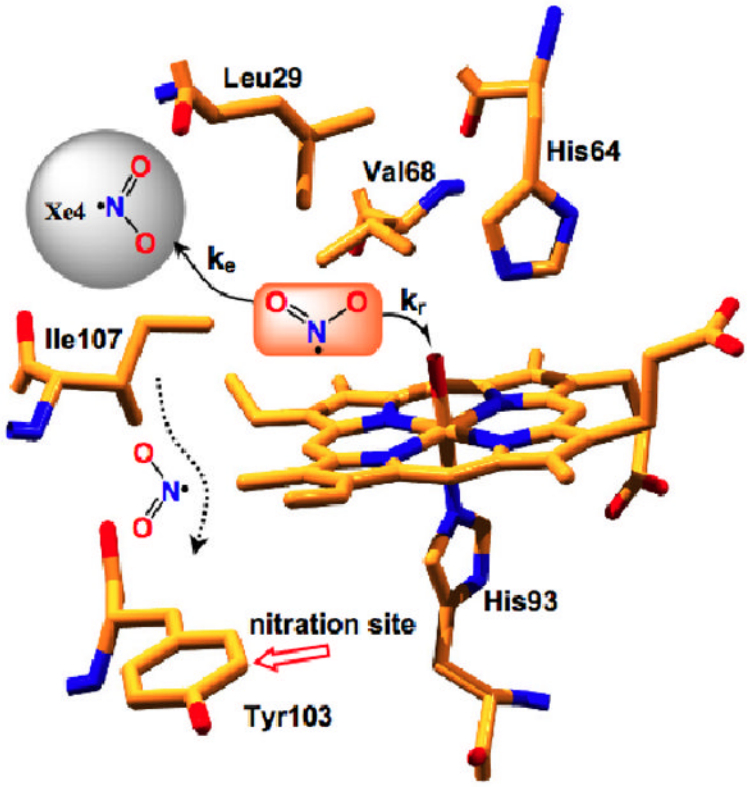

Figure 6.

Proposed distal pocket structure of the caged intermediate [Fe^{IV}=O ·NO_2] in horse heart myoglobin (PDB entry: 2V1F, a myoglobin compound II crystal structure). The caged radical pair [Fe^{IV}=O ·NO_2] is not expected to build up to detectable concentrations due to rapid in-cage rebound (k_r) and cage escape of NO_2 (k_e), which may include the adjacent xenon cavity Xe4. NO_2 that diffuses away from the heme center can induce nitration of Tyr103.

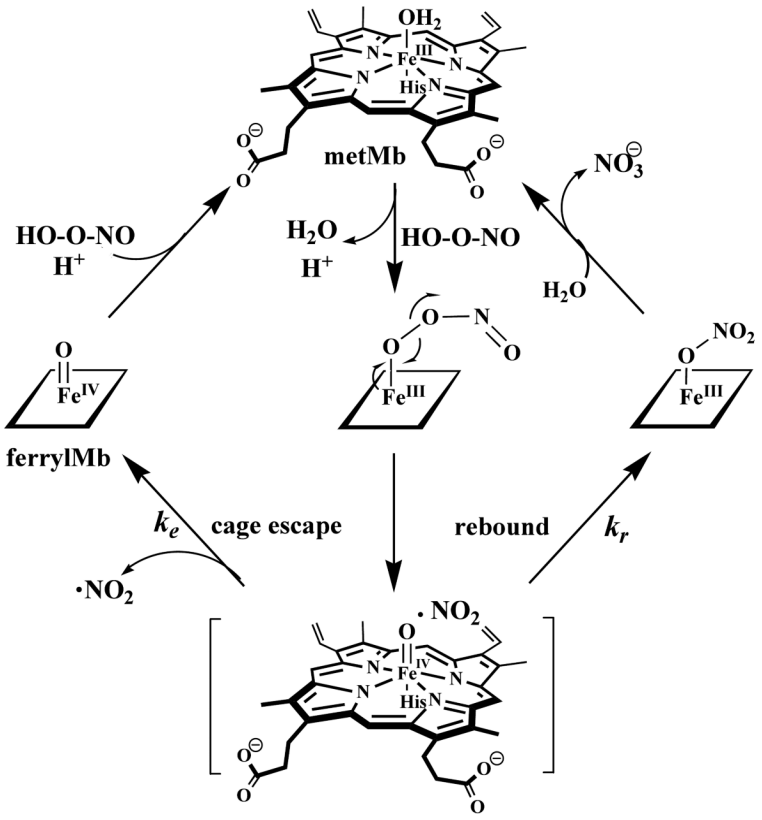

Scheme 1.

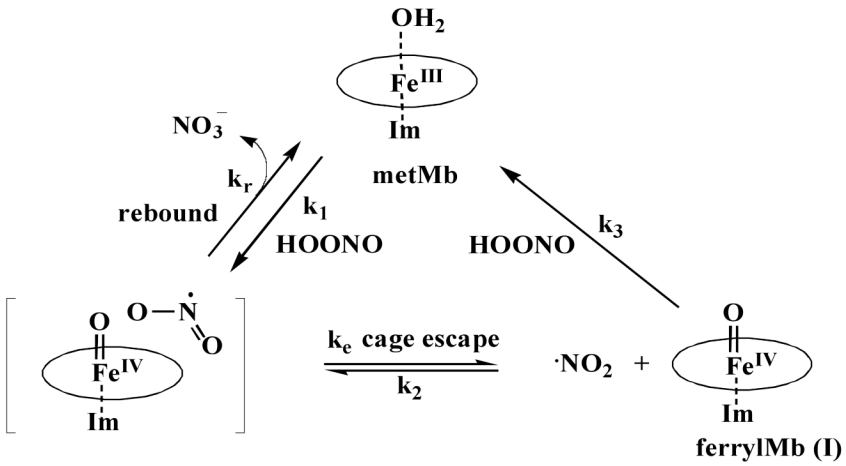

Scheme 2.
The core catalytic cycle of metMb-catalyzed peroxynitrite decay.